ARTICLE

Tracer diffusion in single crystalline CoCrFeNi and CoCrFeMnNi high entropy alloys

Daniel Gaertner,[a] Josua Kottke, Gerhard Wilde, and Sergiy V. Divinski[b]
Institute of Materials Physics, University of Münster, Münster 48149, Germany

Yury Chumlyakov
Department of Physics of Metals, Tomsk State University, Tomsk 634050, Russia

(Received 28 February 2018; accepted 1 May 2018)

High entropy alloys are multicomponent alloys, which consist of five or more elements in equiatomic or nearly equiatomic concentrations. These materials are hypothesized to show significantly decreased self-diffusivities. For the first time, diffusion of all constituent elements in equiatomic CoCrFeNi and CoCrFeMnNi single crystals and additionally solute diffusion of Mn in the quaternary alloy is investigated using the radiotracer technique, thereby the tracer diffusion coefficients of ^{57}Co, ^{51}Cr, ^{59}Fe, ^{54}Mn, and ^{63}Ni are determined at a temperature of 1373 K. The components are characterized by significantly different diffusion rates, with Mn being the fastest element and Ni and Co being the slowest ones. Furthermore, solute diffusion of Cu in the CoCrFeNi single crystal is investigated in the temperature range of 973–1173 K using the ^{64}Cu isotope. In the quaternary alloy, Cu is found to be a fast diffuser at the moderate temperatures below 1273 K and its diffusion rate follows the Arrhenius law with an activation enthalpy of about 149 kJ/mol.

I. INTRODUCTION

High entropy alloys (HEAs) are a new class of multicomponent alloys containing constituents in equiatomic or nearly equiatomic proportions which promise to provide attractive mechanical properties including attractive strength–ductility combinations both at high and low temperatures.[1] Such alloys were believed to be prone to the formation of simple solid solutions instead of complex (and often brittle) intermetallic phases or compounds due to their high configuration mixing entropy (ΔS_{mix}).[2] However, recent studies mention the formation enthalpy between elements as a counterpart to the configurational entropy in determining the phase stability in HEAs. After Zhang et al., the high mixing entropy state does not always have the lowest Gibbs free energy.[3] Furthermore, complex phases may precipitate in HEAs after long annealing treatments, typically at not too high temperatures. Ab initio calculations for the CoCrFeMnNi alloy show that vibrational, electronic, and magnetic contributions to entropy are as well important as the configurational one.[4] Even short annealing at 450 °C of the severe plastically deformed CoCrFeMnNi alloy results in a phase decomposition, suggesting that a high mixing entropy does not guarantee the phase stability.[5,6] Moreover, the single phase observed in HEAs might be a high temperature phase with a kinetically constrained transformation.[5]

In recent years, numerous HEAs have been investigated focusing on high temperature mechanical properties,[7,8] creep strength,[9–12] oxidation resistance,[13–15] and coating applications,[16] following an originally introduced paradigm of four "core effect", i.e., a high entropy, severe lattice distortion, 'cocktail' effect, and sluggish diffusion.[2] Although these basic principles are questioned now,[17,18] the understanding of the diffusion kinetics in HEAs is of fundamental significance. The slow diffusion kinetics is assumed to be responsible for HEAs' unique features like excellent thermal stability, decelerated grain growth, formation of nanoprecipitates,[1] and an excellent resistance to grain coarsening in the nanocrystalline CoCrFeNi alloy.[19] The impact of sluggish diffusion on enhanced creep resistance in the nanocrystalline CoCrFeMnNi alloy has also been discussed.[9]

The present knowledge about diffusion in HEAs is limited to several interdiffusion (applying diffusion couples or multiples) investigations on the one hand[20–22] and the direct radiotracer diffusion measurements in polycrystalline CoCrFeNi and CoCrFeMnNi on the other hand.[23–25] Using a quasi-binary approach (originally called as pseudo-binary one),[26] the interdiffusion coefficients in a CoCrFeMn0.5Ni alloy were determined.[20] The derived values were proposed to be approximately equal to the intrinsic and tracer diffusivities of the equiatomic CoCrFeMnNi alloy with a thermodynamic

Address all correspondence to these authors.
[a]e-mail: daniel.gaertner@wwu.de
[b]e-mail: divin@wwu.de
DOI: 10.1557/jmr.2018.162

factor of about unity.[20] In fact, this assumption was found to be correct in the framework of the random alloy model.[27] The observed low diffusion rates were attributed to a higher normalized activation enthalpy Q/T_m (Q is the activation enthalpy and T_m is the melting temperature) of diffusion in HEAs in comparison to pure metals or corresponding binary and ternary alloys.

Recent interdiffusion experiments revealed an important role of diffusional interactions in HEAs.[21] Moreover, sluggish diffusion has been reported in nonequiatomic AlCrCrFeNi alloys[22] highlighting the importance of the crystallographic parameters (coordination numbers, average interatomic distance, etc.) in determining the diffusion behavior rather than simply attributing it to the varying chemical environments.

Although the first diffusion couple experiments seemed to support the paradigm about "sluggish diffusion",[20] recent direct (radio)tracer self-diffusion experiments in equiatomic CoCrFeNi and CoCrFeMnNi polycrystalline HEAs verified that diffusion in HEAs is not inevitably sluggish.[23,25] It may become apparently sluggish in fcc systems if considered at a given homologous temperature. However, the diffusion measurements on polycrystalline samples were complicated by the presence of a second contribution which was identified with enhanced (short-circuit) grain boundary diffusion.[23] Astonishingly, a strong contribution of grain boundary diffusion was observed even in a coarse-grained material (grain size >200 μm) at temperatures about $0.8T_m$ for a relatively slow diffusing species like Ni![23] Tracer diffusion measurements in single crystalline materials are required to provide the true volume diffusion data and to verify the correctness of the profile analysis on polycrystalline counterparts.

In the present work, the results of the first tracer self-diffusion measurements in equiatomic CoCrFeNi and CoCrFeMnNi single crystal HEAs are reported fully supporting the published previously diffusion data on polycrystalline CoCrFeNi and CoCrFeMnNi HEAs[23,25] at a temperature of 1373 K. Furthermore, solute diffusion of Cu and Mn in the same CoCrFeNi single crystals is investigated.

II. EXPERIMENTAL PROCEDURE

A. Sample preparation

CoCrFeNi and CoCrFeMnNi single crystals (each ⟨001⟩- and ⟨111⟩-oriented) with a diameter of 24 mm and a length of about 10 cm were grown using the modified Bridgman technique under a purified Ar atmosphere with a slight surplus of Mn. The single crystals were carefully etched first and then homogenized at 1473 K for 50 h followed by quenching in oil. Subsequently, cylindrical samples of 8 mm in diameter were cut and sliced in discs of a thickness of 1.5 mm by spark-erosion and again etched carefully with aqua regia. One face of the specimen was polished by a standard metallographic procedure to a mirror-like quality. Finally, the prepared samples were sealed in a silica glass tube under a purified (5 N) Ar atmosphere, annealed at 1373 K for 3 days and quenched in air to room temperature. This procedure produced a homogeneous microstructure with an equilibrium concentration of point defects at the temperature of subsequent diffusion measurements.

B. Radiotracer experiments

The radiotracers ^{57}Co, ^{51}Cr, ^{59}Fe, ^{54}Mn, and ^{63}Ni were available as HCl solutions. The original solutions were highly diluted with double-distilled water achieving the required specific activity of the tracer material. The mixture of tracers (^{57}Co + ^{51}Cr + ^{59}Fe + ^{54}Mn, with the radioactivity of about 5 kBq for each tracer) was applied on the polished sample surface and dried. Since the ^{63}Ni isotope is a purely β-emitter, it was applied separately on identical samples to avoid difficulties in determination of the corresponding decay activities via energy discrimination. The radioactivities of all other isotopes could conveniently be determined via energy discrimination by gamma spectrometry.

Under a purified Ar atmosphere, the samples were sealed into silica glass tubes and subjected to diffusion annealing at a temperature of 1373 K for the chosen times. The temperature was measured and controlled by a Ni–NiCr thermocouple to an accuracy of ±1 K. To remove the effects of lateral and surface diffusion, the samples were reduced in diameter by about 1–2 mm. The penetration profiles were determined by precise parallel mechanical sectioning using a grinding machine and grinding paper with SiC grains of about 30 μm. The section masses were determined by weighing the samples before and after sectioning on a microbalance to an accuracy of 10^{-4} mg.

To measure the activity of each section, an available pure Ge γ-detector equipped with a 16 K multichannel analyzer was used. The radioisotopes ^{57}Co, ^{51}Cr, ^{59}Fe, and ^{54}Mn decay emitting γ-quanta whose energies (listed in Table I) can easily be distinguished by the available setup.

Since the ^{63}Ni radioisotope (half-life 101.2 years) is a β^--emitter, it can conveniently be analyzed separately using a liquid scintillation counter (a LSC-detector

TABLE I. γ-quanta emitting radiotracers used in the experiments.

Isotope	Half-life (d)	Energy (keV)	Ref.
^{57}Co	271.7	122.1 136.5	28
^{51}Cr	27.7	320.1	29
^{59}Fe	44.5	1099.2 1291.6	30
^{54}Mn	312.2	834.8	31

https://doi.org/10.1557/jmr.2018.162

TRI-CARB 2910, Perkin Elmer, Waltham, Massachusetts, was used).

The ^{64}Cu isotope was available as a beam, provided by the ISOLDE (Isotope Separator On-Line Device) radioactive beam facility at CERN. Approximately 10^{11} atoms were implanted at the mean depth of about 17 nm (as simulated using SRIM—Stopping and Range of Ions in Matter—software[32]) into the CoCrFeNi single crystals. Since the ^{64}Cu isotope has a very short half-life, 12.7 h,[33] the samples were annealed under high vacuum in a temperature range of 973–1173 K for the chosen times using an on-line diffusion chamber.[34] In the same diffusion chamber, the penetration profiles were determined by ion-beam sputtering using an Ar-ion beam. The positrons emitted as β^+-decays can be analyzed observing the 511 keV peak using an available NaJ γ-detector with a 16 K multichannel analyzer. The penetration depth can be estimated by the mass difference of the sample before and after the whole experiment using a microbalance and assuming a constant sputtering rate. During sputtering, the beam current was recorded and proven to be constant within $\pm 5\%$.

III. EXPERIMENTAL RESULTS AND DISCUSSION

A. Microstructure analysis

To check the orientation, sub-grain structure and the chemical composition of the single crystals, orientation imaging microscopy using electron backscatter diffraction (EBSD), and energy dispersive X-ray spectroscopy (EDX) were applied. As an example, Fig. 1 shows the grain orientation mapping using the inverse pole figure (inset) and the chemical maps obtained for the ⟨001⟩-oriented CoCrFeMnNi crystal. The EBSD analysis of both alloys confirms the expected orientations of the single crystals. Furthermore, the chemical maps and the dedicated EDX analysis (Table II) verify the homogeneity and the equiatomic composition for both alloys. Small, micrometer large Cr- (in CoCrFeNi) or Mn-rich (in CoCrFeMnNi) precipitates could occasionally be found. Their volume fraction is small and should not affect the intended diffusion measurements. The precipitates may appear during single crystal preparation via the Bridgman technique or the subsequent heat treatment. Sub-grain boundaries with the misorientation less than 2° were observed, too, and the sub-grain size was found to be larger than 500 μm. Thus, the samples represent single crystals suitable for volume diffusion measurements.

B. Tracer measurements

The radiotracer experiments were performed at 1373 K for significantly different diffusion times (6 h, 3 days, and 14 days) applying small amount of the isotope mixtures and ensuring thus the instantaneous source initial conditions. Then, the tracer concentration has to follow a thin film solution of the diffusion problem,[35]

$$\bar{c}(y,t) = \frac{M_0}{\sqrt{\pi D_V t}} \exp\left(-\frac{y^2}{4D_V t}\right) \quad , \qquad (1)$$

with M_0 being the initial tracer amount, $\bar{c}$ being the relative specific activity of the layer, which is proportional to the solute concentration, y being the penetration depth, t being the diffusion time, and D_V being the volume diffusion coefficient. In Fig. 2(a), the measured profiles for Co diffusion in both alloys along the ⟨001⟩ direction are exemplarily shown. Except few very first points, the concentration profiles do follow the Gaussian solution, Eq. (1), over two to three orders of magnitude in the decrease of the tracer concentration with unexpected

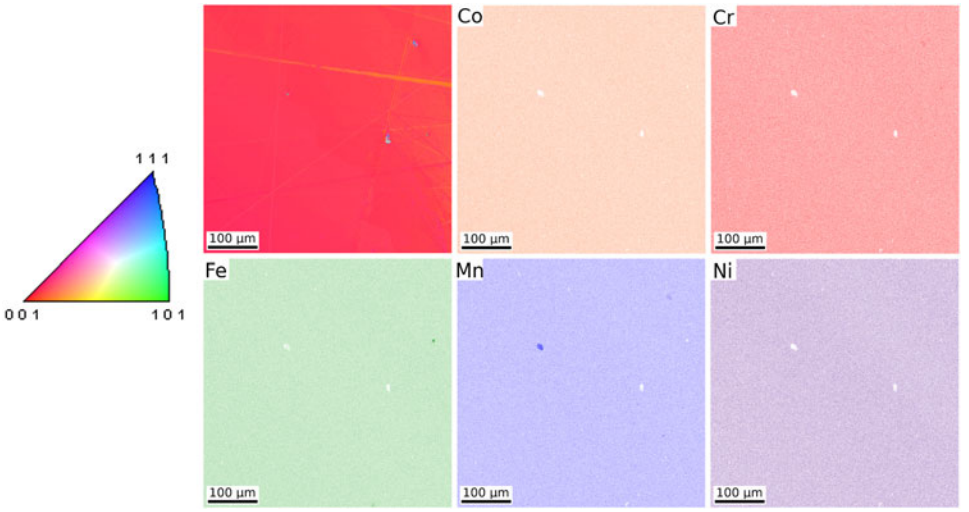

FIG. 1. Orientation imaging microscopy of the ⟨001⟩ CoCrFeMnNi single crystal and the corresponding elemental maps obtained by EDX analysis. The grain orientations are colored according to the inverse pole figure (left panel).

deviations at low activities, which are still definitely higher than the background values, estimated at about 0.02 Bq/mg for the chosen counting conditions. The second, fast-diffusion branches are seen almost for all penetration profiles irrespective of the diffusion direction. Most probably, they correspond to enhanced pipe diffusion. Note that the dislocation walls as sub-grain boundaries were found by the EBSD analysis. For a precise analysis, a detailed characterization of the samples with respect to the dislocation density and their geometric configurations is required and it is a subject of ongoing work. In the present report, we focused on the volume diffusion branches which dominate the tracer distribution, as shown in Fig. 2(a).

In Fig. 2(b), the penetration profiles measured for Fe diffusion in both alloys at 1373 K for the different diffusion times are exemplarily plotted using the normalized coordinates, $\ln \bar{c} \cdot \sqrt{t}$ versus y^2/t, which should provide a unified, "master" plot for the instantaneous source initial conditions and a constant (time-independent) volume diffusion coefficient,[36] see Eq. (1). The present data verify that the volume diffusion coefficients of all constituting elements in the single crystalline CoCrFeNi and CoCrFeMnNi alloys are time-independent (the determined volume diffusion coefficients, D_V, of each element deviate maximum 50% from the average values; see Fig. 5.) and isotropic as it is expected for the crystals with a cubic symmetry. Note that the time-dependent diffusion experiments should help to establish the nature of the fast-diffusion branches in the concentration profiles. The normalized penetration profiles are not perfectly overlapping due to inherent difficulties to ensure the same tracer amount applied to all the samples, but the differences are within a factor of two.

In Figs. 3(a) and 3(b), the first branches of the penetration profiles measured correspondingly in the CoCrFeNi and CoCrFeMnNi single crystals as a result of diffusion for 3 days are shown against the penetration depth squared. The concentration profiles measured in the ⟨001⟩- and ⟨111⟩-orientated single crystals are shown by the filled and open symbols, respectively. The solid lines in Fig. 3 represent the expected Gaussian solutions in the pertinent coordinates. As a result, the tracer volume diffusion coefficients, D_V, can be determined from the slopes of the corresponding lines,

$$D_V = \frac{1}{4t}\left(-\frac{\partial \ln \bar{c}}{\partial y^2}\right)^{-1} \quad . \qquad (2)$$

Depending on diffusion time applied, the concentration profiles could be followed to the penetration depths from several ten up to several hundred micrometers. All relevant parameters of the diffusion experiments and the determined diffusion coefficients are summarized in Tables III and IV for CoCrFeNi and CoCrFeMnNi HEAs, respectively.

TABLE II. Composition (in at.%) of CoCrFeNi and CoCrFeMnNi crystals as determined by EDX analysis. The uncertainty of concentrations is less than ±0.2%.

Alloy	Co	Cr	Fe	Mn	Ni
CoCrFeNi	25.1	24.9	25.2	. . .	24.8
CoCrFeMnNi	19.9	19.4	19.6	20.2	20.9

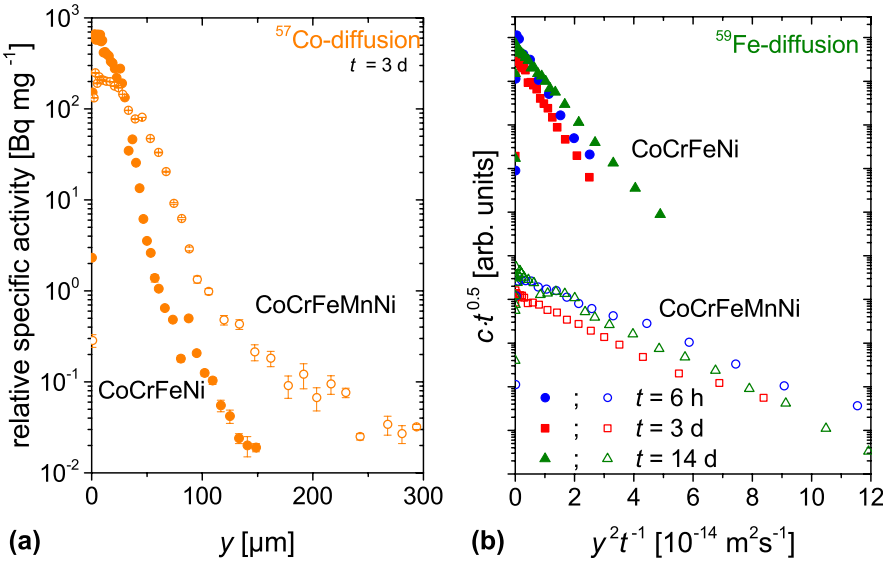

FIG. 2. Penetration profiles measured at 1373 K (a) for Co-diffusion for 3 days and (b) for Fe-diffusion for several diffusion times along the ⟨001⟩ direction in both CoCrFeNi and CoCrFeMnNi HEAs. In (b), the normalized coordinates $\ln \bar{c} \cdot \sqrt{t}$ and y^2/t are used and the concentration profiles measured in CoCrFeNi are shifted along the ordinate axis for a better visualization. $\bar{c}$ is the layered tracer concentration, y is the penetration depth, and t is the diffusion time. In (a) and (b), the filled (open) symbols correspond to CoCrFeNi (CoCrFeMnNi).

https://doi.org/10.1557/jmr.2018.162

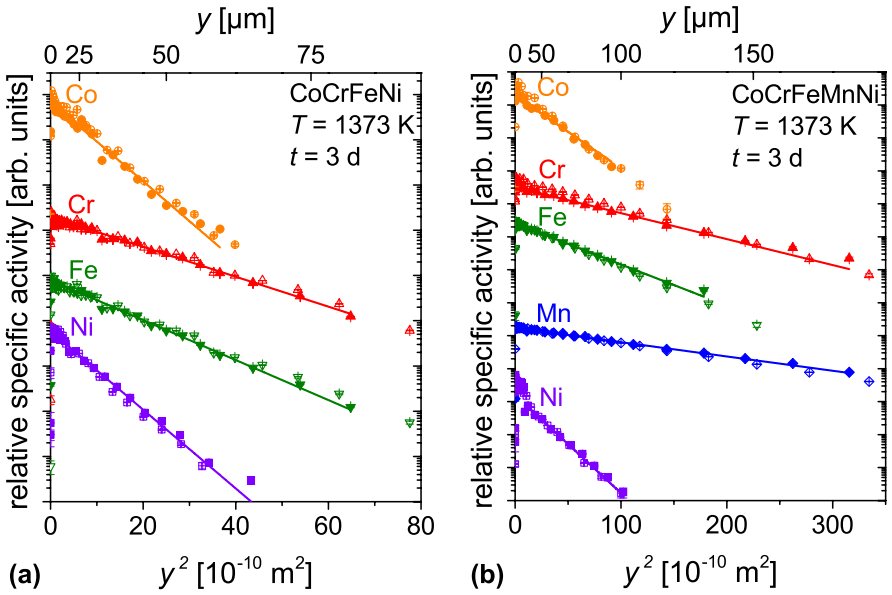

FIG. 3. Penetration profiles measured after diffusion at 1373 K for 3 days in CoCrFeNi (a) and in CoCrFeMnNi single crystals. (b) y is the penetration depth. In (a) and (b), the filled (open) symbols indicate the profiles measured in crystals with the ⟨001⟩ (⟨111⟩) orientation.

TABLE III. Diffusion time t and the determined tracer diffusion coefficients D_V in CoCrFeNi single crystal HEAs at 1373 K. The uncertainty of the D_V values is typically below 20%.

Element	Orientation	t 10^5 s	D_V 10^{-15} m^2/s	$\sqrt{D_V t}$ μm
Co	⟨001⟩	2.6	0.46	11
	⟨111⟩	2.6	0.47	11
	⟨001⟩	12	0.64	24
Cr	⟨111⟩	0.22	2.8	7.8
	⟨001⟩	2.6	1.3	18
	⟨111⟩	2.6	1.4	19
	⟨001⟩	12	2.4	54
Fe	⟨001⟩	0.22	0.98	4.6
	⟨001⟩	2.6	0.95	16
	⟨111⟩	2.6	1.0	16
	⟨001⟩	12	1.4	41
Mn	⟨001⟩	12	3.2	62
Ni	⟨001⟩	2.6	0.49	11
	⟨111⟩	2.6	0.42	10

TABLE IV. Diffusion time t and the determined tracer diffusion coefficients D_V in CoCrFeMnNi single crystal HEAs at 1373 K. The uncertainty of the D_V values is typically below 20%.

Element	Orientation	t 10^5 s	D_V 10^{-15} m^2/s	$\sqrt{D_V t}$ μm
Co	⟨001⟩	0.22	2.5	7.3
	⟨001⟩	2.6	1.9	22
	⟨111⟩	2.6	1.4	19
	⟨001⟩	12	1.6	44
Cr	⟨001⟩	0.22	6.3	12
	⟨001⟩	2.6	5.3	37
	⟨111⟩	2.6	4.8	35
	⟨001⟩	12	4.6	75
Fe	⟨001⟩	0.22	4.1	9.4
	⟨001⟩	2.6	3.4	30
	⟨111⟩	2.6	3.1	28
	⟨001⟩	12	3.2	62
Mn	⟨001⟩	0.22	11.0	15
	⟨001⟩	2.6	9.7	50
	⟨111⟩	2.6	8.6	47
	⟨001⟩	12	7.4	95
Ni	⟨001⟩	2.6	1.4	19
	⟨111⟩	2.6	1.1	17

Figure 5 shows an Arrhenius representation of the measured diffusion coefficients in single crystalline alloys in comparison to the self-diffusion data determined previously in the polycrystalline quaternary and quinary HEAs.[23,25] The homologous temperature scale, i.e., normalized on the melting temperatures of the investigated HEAs, is used. The melting temperatures of both HEAs were determined in Ref. 23. The single crystal data are in a very good agreement with the Arrhenius data established previously for the polycrystalline material.

In the quaternary alloy, Co and Ni diffusion coefficients measured in single crystalline alloys are slightly higher than the corresponding polycrystalline data that could be explained by strong contributions of grain boundary diffusion in the latter that hindered a reliable extraction of the volume diffusion data. However, the deviations of single crystalline and polycrystalline data are not significant and do not exceed 20% that can be considered as satisfactory.

For a first time, the diffusion of Mn as a solute in CoCrFeNi is measured and it is found that Mn is

the fastest element in the quaternary alloy at 1373 K. Tables III and IV suggest further that the diffusion rates of all investigated elements are increased after alloying of the quartenary alloy by Mn, keeping an equiatomic ratio of the elements, when compared at the same absolute temperature. If compared on the homologous temperature scale, diffusion in 4-component HEA is generally faster than that in the 5-component alloy at lower temperatures and the relationship is reversed at higher temperatures near the melting point, as shown in Fig. 5. The present results support fully the corresponding findings in polycrystalline materials[23,25] and verify unambiguously that the diffusion in HEAs is not a priori sluggish.

C. Cu diffusion

The diffusion experiments with implanted ^{64}Cu tracer atoms were performed at 3 different temperatures in a range of 973–1173 K. Figure 4 presents the concentration profiles including a "zero" profile (black squares) as a function of the penetration depth. The zero profile was determined by ion-beam sputtering directly after implantation without any heat treatment of the sample in order to check the depth resolution and quantify the ion-beam–induced mixing. The resulting tracer distribution is characterized by a high near-surface activity followed by an abrupt drop of the tracer concentration to the background level at about 1 Bq/mg. Thus, the determined profiles do represent the true tracer diffusion of Cu atoms in the single crystalline alloy.

The tracer concentration decreases following approximately the Gaussian solution of the diffusion problem, Eq. (1), beginning at depths of several hundred nanometers. However, the tracer atoms were implanted to the depths of about 17 nm, so the maximum tracer concentration was expected in the first sectioned layer of the sample. Such a behavior was already observed measuring, e.g., potassium self-diffusion in single crystalline alkali feldspar,[37] and it is explained by the tracer evaporation at the external surface under vacuum conditions. Including the influence of distinctly increasing tracer concentration at the beginning of the penetration profiles, the volume diffusion coefficients, D_V, can be determined using Strohm's solution[38] (solid lines in Fig. 4),

$$\bar{c}(y,t) = \frac{M_0/2}{\sqrt{1+(2D_V t/\sigma^2)}} \cdot \left[\operatorname{erfc}\left(\frac{-(y_0/2\sigma^2)-(y/4D_V)}{\sqrt{(1/2\sigma^2)+(1/4D_V)}} \right) \cdot \exp\left(\frac{-(y-y_0)^2}{2\sigma^2+4D_V t} \right) + k \operatorname{erfc}\left(\frac{-(y_0/2\sigma^2)+(y/4D_V)}{\sqrt{(1/2\sigma^2)+(1/4D_V)}} \right) \cdot \exp\left(\frac{-(y+y_0)^2}{2\sigma^2+4D_V t} \right) \right] \quad . \tag{3}$$

Here, M_0 is the maximum relative specific activity, y_0 is the implantation depth, and σ^2 is the width of the implanted tracer distribution. The factor k accounts for the surface conditions: $k = +1$ if the surface is a perfect reflector for the diffusing atoms and $k = -1$ if the surface is a perfect sink. The values of k between these two limits, i.e., $-1 < k < +1$, represent some intermediate situation. All relevant parameters of the diffusion experiments and the determined diffusion coefficients are summarized in Table V. In all measurements the value k was found to be approximately -1, so the sample surface acted as a perfect sink for the tracer atoms during the diffusion annealing treatments at high-vacuum conditions. The measured diffusion coefficients are plotted in Fig. 5. Diffusion of Cu as a solute in CoCrFeNi is found to follow the Arrhenius dependence,

$$D_V^{Cu} = \left(6.6^{+19.5}_{-5.0}\right) \times 10^{-10} \cdot \exp\left(-\frac{(149.9 \pm 12.1)\text{kJ/mol}}{RT} \right) \text{m}^2/\text{s} \quad . \tag{4}$$

Figure 5 substantiates that in the investigated temperature range, Cu atoms diffuse faster in the quaternary HEA than all constituting elements, Co, Cr, Fe, and Ni, with an astonishingly smaller activation energy, by a factor of two. For example, the pre-exponential factor D_0 of Cu diffusion is about three orders of magnitude lower than that for Co and the activation enthalpy is about 50% smaller. With increasing temperature up to 1373 K ($0.8T_m$), the Cu diffusion rates would correspond to those of Fe atoms and would be lower than those of Cr and Mn.

Following the Le Claire model of impurity diffusion in fcc metals,[39] one may suggest a strong attractive

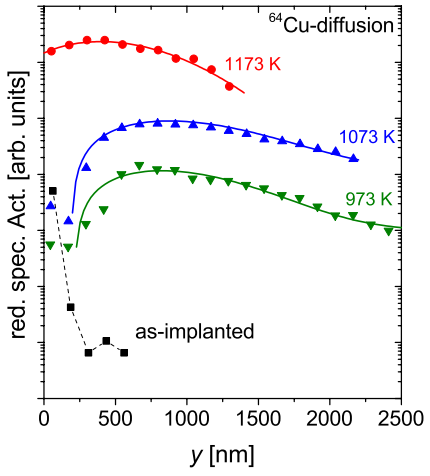

FIG. 4. Penetration profiles measured for Cu diffusion in single crystalline CoCrFeNi at different temperatures. The black squares represent the profile measured directly after implantation without any heat treatment. The solid lines correspond to the fits by Eq. (3). y is the penetration depth.

TABLE V. Experimental parameters (temperature T and time t) and the determined diffusion coefficients D_V for ^{64}Cu diffusion in CoCrFeNi single crystals. The uncertainty of the D_V values is typically below 20%.

T (K)	t (s)	D_V (m^2/s)	$\sqrt{D_V t}$ (nm)
973	43,200	5.6×10^{-18}	490
1073	7200	3.9×10^{-17}	530
1173	1200	1.3×10^{-16}	390

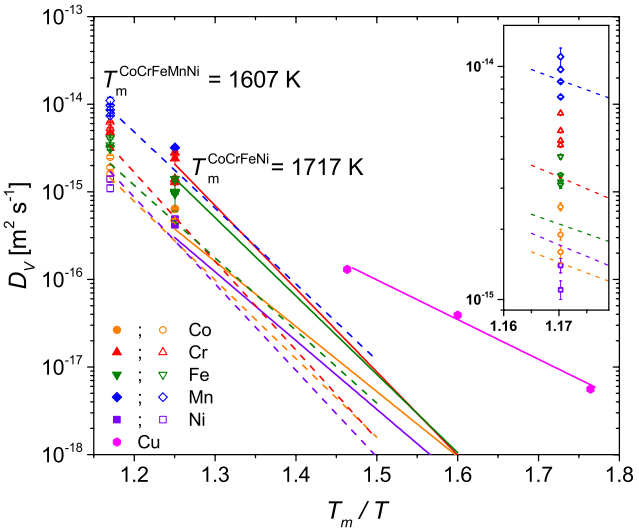

FIG. 5. Co, Cr, Fe, Mn, and Ni tracer diffusion coefficients in HEA single crystals (filled symbols correspond to CoCrFeNi and open symbols correspond to CoCrFeMnNi) in comparison to the Arrhenius plots established for self-diffusion in polycrystalline counterparts (straight lines correspond to CoCrFeNi and dashed lines correspond to CoCrFeMnNi)[23,25] and Cu solute diffusion in the CoCrFeNi HEA single crystals (pink hexagons and pink straight line). The inset magnifies the data points measured in CoCrFeMnNi.

interaction of Cu atoms with vacancies in the HEAs of transition metal elements. This finding would indicate a facilitated precipitation of Cu-rich particles in CoCrFeNi. Whether these results could be transferred to another systems, e.g., CoCrCuFeNi and AlCoCrCuFeNi HEAs, is still an open question, especially in view of complex fcc + bcc crystal structures of AlCoCrCuFeNi.[40]

IV. SUMMARY

In the present work, self-diffusion (of Co, Cr, Fe, and Ni) and solute diffusion of Mn and Cu in CoCrFeNi are measured for the first time in equiatomic HEA single crystals. The self-diffusion coefficients are in good agreement with the previously reported data on polycrystalline equiatomic HEAs, providing the true volume diffusion data without any interference with the grain boundary diffusion flux. Mn tends to be the fastest diffuser in the quaternary and quinary alloys. Diffusion in HEAs is not retarded after further alloying of the quaternary CoCrFeNi HEA by Mn to the quinary CoCrFeMnNi alloy if compared at a given absolute temperature. Thus, the present measurements do not support a historically invented statement on "sluggish" diffusion as a core effect in HEAs. A change of the paradigm is required.

The temperature dependence of Cu tracer diffusion in the quaternary HEA follows an Arrhenius behavior in a temperature range between 973–1173 K with an activation enthalpy of about 149 kJ/mol, which is about 50% lower than the activation enthalpies of the other measured elements. Cu is found to diffuse fast in the investigated temperature range that indicates an attractive interaction with vacancies in the transition metal atom HEA.

ACKNOWLEDGMENTS

Financial support by the Deutsche Forschungsgemeinschaft (DFG) (research Project No. DI 1419/13-1) is gratefully acknowledged. The usage of implantation equipment supported by the Federal Ministry of Education and Research (BMBF) through Grant Nos. 05K13MG1 and 05K16PGA (ISOLDE Project Nos. IS626 & IS627) is gratefully acknowledged. We would like to express our special thanks to the support by the ISOLDE team (particularly Fabian Hergemöller, Juliana Schell, Karl Johnston, and João Guilherme Correia).

REFERENCES

1. B.S. Murty, J.W. Yeh, and S. Ranganathan: *High Entropy Alloys* (Elsevier, London, 2014).
2. J.W. Yeh, S.K. Chen, S.J. Lin, J.Y. Gan, T.S. Chin, T.T. Shun, C.H. Tsau, and S.Y. Chang: Nanostructured high-entropy alloys with multiple principal elements: Novel alloy design concepts and outcomes. *Adv. Eng. Mater* **6**, 299–303 (2004).
3. F. Zhang, C. Zhang, S.K. Chen, J. Zhu, W.S. Cao, and U.R. Kattner: An understanding of high entropy alloys from phase diagram calculations. *Calphad* **45**, 1–10 (2014).
4. D. Ma, B. Grabowski, F. Körmann, J. Neugebauer, and D. Raabe: Ab initio thermodynamics of the CoCrFeMnNi high entropy alloy: Importance of entropy contributions beyond the configurational one. *Acta Mater* **100**, 90–97 (2015).
5. B. Schuh, F. Mendez-Martin, B. Völker, E.P. George, H. Clemens, R. Pippan, and A. Hohenwarter: Mechanical properties, microstructure and thermal stability of a nanocrystalline CoCrFeMnNi high-entropy alloy after severe plastic deformation. *Acta Mater* **96**, 258–268 (2015).
6. F. Otto, A. Dlouhý, K.G. Pradeep, M. Kubenová, D. Raabe, G. Eggeler, and E.P. George: Decomposition of the single-phase high-entropy alloy CrMnFeCoNi after prolonged anneals at intermediate temperatures. *Acta Mater* **112**, 40–52 (2016).
7. N.N. Guo, L. Wang, L.S. Luo, X.Z. Li, R.R. Chen, Y.Q. Su, J.J. Guo, and H.Z. Fu: Hot deformation characteristics and dynamic recrystallization of the MoNbHfZrTi refractory high-entropy alloy. *Mater. Sci. Eng., A* **651**, 698–707 (2016).
8. H. Chen, A. Kauffmann, B. Gorr, D. Schliephake, C. Seemüller, J.N. Wagner, H-J. Christ, and M. Heilmaier: Microstructure and mechanical properties at elevated temperatures of a new

Al-containing refractory high-entropy alloy Nb–Mo–Cr–Ti–Al. *J. Alloys Compd* **661**, 206–215 (2016).
9. D.H. Lee, M.Y. Seok, Y. Zhai, I.C. Choi, J. He, Z. Lu, J.Y. Suh, U. Ramamurty, M. Kawasaki, T.G. Langdon, and J.I. Jang: Spherical nanoindentation creep behavior of nanocrystalline and coarse-grained CoCrFeMnNi high-entropy alloys. *Acta Mater* **109**, 314–322 (2016).
10. L. Zhang, P. Yu, H. Cheng, H. Zhang, H. Diao, Y. Shi, B. Chen, P. Chen, R. Feng, J. Bai, Q. Jing, M. Ma, P.K. Liaw, G. Li, and R. Liu: Nanoindentation creep behavior of an $Al_{0.3}$CoCrFeNi high-entropy alloy. *Metall. Mater. Trans. A* **47**, 1–5 (2016).
11. Y. Ma, Y.H. Feng, T.T. Debela, G.J. Peng, and T.H. Zhang: Nanoindentation study on the creep characteristics of high-entropy alloy films: Fcc versus bcc structures. *Int. J. Refract. Met. Hard Mater.* **54**, 395–400 (2016).
12. T. Cao, J. Shang, J. Zhao, C. Cheng, R. Wang, and H. Wang: The influence of Al elements on the structure and the creep behavior of Al_xCoCrFeNi high entropy alloys. *Mater. Lett.* **164**, 344–347 (2016).
13. W. Kai, C.C. Li, F.P. Cheng, K.P. Chu, R.T. Huang, L.W. Tsay, and J.J. Kai: The oxidation behavior of an equimolar FeCoNiCrMn high-entropy alloy at 950 °C in various oxygen-containing atmospheres. *Corros. Sci.* **108**, 209–214 (2016).
14. G. Laplanche, U.F. Volkert, G. Eggeler, and E.P. George: Oxidation behavior of the CrMnFeCoNi high-entropy alloy. *Oxid. Met* **85**, 629–645 (2016).
15. G.R. Holcomb, J. Tylczak, and C. Carney: Oxidation of CoCrFeMnNi high entropy alloys. *JOM* **67**, 2326–2339 (2015).
16. R.A. Shaginyan, N.A. Krapivka, S.A. Firstov, N.I. Danilenko, and I.V. Serdyuk: Superhard vacuum coatings based on high-entropy alloys. *Powder Metall. Met. Ceram.* **54**, 725–730 (2016).
17. E.J. Pickering and N.G. Jones: High-entropy alloys: A critical assessment of their founding principles and future prospects. *Int. Mater. Rev.* **61**, 1–20 (2016).
18. D.B. Miracle: High-entropy alloys: A current evaluation of founding ideas and core effects and exploring "nonlinear alloys". *JOM* **69**, 2130–2136 (2017).
19. S. Praveen, J. Basu, S. Kashyap, and R.S. Kottada: Exceptional resistance to grain growth in nanocrystalline CoCrFeNi high entropy alloy at high homologous temperatures. *J. Alloys Compd* **662**, 361–367 (2016).
20. K.Y. Tsai, M.H. Tsai, and J.W. Yeh: Sluggish diffusion in Co–Cr–Fe–Mn–Ni high-entropy alloys. *Acta Mater* **61**, 4887–4897 (2013).
21. K. Kulkarni and G.P.S. Chauhan: Investigations of quaternary interdiffusion in a constituent system of high entropy alloys. *AIP Adv.* **5**, 097162 (2015).
22. J. Dabrowa, W. Kucza, G. Cieslak, T. Kulik, M. Danielewski, and J.W. Yeh: Interdiffusion in the fcc-structured Al–Co–Cr–Fe–Ni high entropy alloys: Experimental studies and numerical simulations. *J. Alloys Compd* **674**, 455–462 (2016).
23. M. Vaidya, S. Trubel, B.S. Murty, G. Wilde, and S.V. Divinski: Ni tracer diffusion in CoCrFeNi and CoCrFeMnNi high entropy alloys. *J. Alloys Compd.* **688**, 994–1001 (2016).
24. M. Vaidya, K.G. Pradeep, B.S. Murty, G. Wilde, and S.V. Divinski: Radioactive isotopes reveal a non sluggish kinetics of grain boundary diffusion in high entropy alloys. *Scientific Reports* **7**, 12273 (2017).
25. M. Vaidya, K.G. Pradeep, B.S. Murty, G. Wilde, and S.V. Divinski: Bulk tracer diffusion in CoCrFeNi and CoCrFeMnNi high entropy alloys. *Acta Mater* **146**, 211–224 (2018).
26. A. Paul: A pseudobinary approach to study interdiffusion and the Kirkendall effect in multicomponent systems. *Philos. Mag* **93**, 2297–2315 (2013).
27. T.R. Paul, I.V. Belova, and G.E. Murch: Analysis of diffusion in high entropy alloys. *Mater Chem Phys* **210**, 301–308 (2018).
28. H.R. Lemmer, O.J.A. Segaert, and M.A. Grace: The decay of cobalt 57. *Proc. Phys. Soc., London, Sect. A* **68**, 701–708 (1955).
29. S. Ofer and R. Wiener: Decay of Cr 51. *Phys. Rev.* **107**, 1639–1641 (1957).
30. R.L. Heath, C.W. Reich, and D.G. Proctor: Decay of 45-day Fe 59. *Phys. Rev.* **118**, 1082 (1960).
31. C.M. Lederer and V.S. Shirley: *Table of Isotopes*, 7th ed. (Wiley, New York, 1978).
32. J.F. Ziegler, D. Ziegler, and J.P. Biersack: SRIM–The stopping and range of ions in matter. *Nucl. Instrum. Methods Phys. Res., Sect. B* **268**, 1818–1823 (2010).
33. M.-M. Bé, V. Chisté, C. dulieu, X. Mougeot, V.P. Chechev, N.K. Kuzmenko, F.G. Kondev, A. Luca, M. Galán, A.L. Nichols, A. Arinc, A. Pearce, X. Huang, B. Wang: *Table of Radionuclides*, Vol. 6 - A = 22 to 242. (Bureau International Des Poids Et Mesures, Sèvres Cedex, France, 2011); pp. 13–18.
34. H. Wolf, F. Wagner, and T. Wichert: Isolde collaboration, anomalous diffusion profiles of Ag in CdTe due to chemical self-diffusion. *Phys. Rev. Lett.* **94**, 125901 (2005).
35. H. Mehrer: *Diffusion in Solids: Fundamentals, Methods, Materials, Diffusion-Controlled Processes* (Springer, Berlin, 2007); p. 53.
36. A. Paul, T. Laurila, V. Vuorinen, and S. Divinski: *Themodynamics, Diffusion and Kirkendall Effect in Solids* (Springer, Switzerland, 2014).
37. F. Hergemöller, M. Wegner, M. Deicher, H. Wolf, F. Brenner, H. Hutter, R. Abart, and N.A. Stolwijk: Potassium self-diffusion in a K-rich single-crystal alkali feldspar. *Phys. Chem. Miner.* **44**, 345–351 (2017).
38. A. Strohm, T. Voss, W. Frank, P. Laitinen, and J. Räisänen: Self-diffusion of ^{71}Ge and ^{31}Si in Si–Ge alloys. *Z. Metallkd.* **93**, 737–744 (2002).
39. A.D. Le Claire: On the theory of impurity diffusion in metals. *Philos. Mag.* **7**, 141–167 (1962).
40. J. Dabrowa, G. Cieslak, M. Stygar, K. Mroczka, K. Berent, T. Kulik, and M. Danielewski: Influence of Cu content on high temperature oxidation behavior of $AlCoCrCu_xFeNi$ high entropy alloys (x = 0, 0.5, 1). *Intermetallics* **84**, 52–61 (2017).